Assessing multiscale Discrete Fracture Network flow with graphs

Diane Doolaeghe, Philippe Davy, Caroline Darcel, Romain Le Goc, Jeffrey De'Haven Hyman

▶ **To cite this version:**

Diane Doolaeghe, Philippe Davy, Caroline Darcel, Romain Le Goc, Jeffrey De'Haven Hyman. Assessing multiscale Discrete Fracture Network flow with graphs. 55th US Rock Mechanics/Geomechanics Symposium., American Rock Mechanics Association (ARMA), Jun 2021, online, United States. insu-03326686

HAL Id: insu-03326686
https://insu.hal.science/insu-03326686

Submitted on 9 Sep 2021

HAL is a multi-disciplinary open access archive for the deposit and dissemination of scientific research documents, whether they are published or not. The documents may come from teaching and research institutions in France or abroad, or from public or private research centers.

L'archive ouverte pluridisciplinaire **HAL**, est destinée au dépôt et à la diffusion de documents scientifiques de niveau recherche, publiés ou non, émanant des établissements d'enseignement et de recherche français ou étrangers, des laboratoires publics ou privés.

ResearchGate

See discussions, stats, and author profiles for this publication at: https://www.researchgate.net/publication/354126561

Assessing multiscale Discrete Fracture Network flow with graphs

Conference Paper · June 2021

CITATIONS
0

READS
32

5 authors, including:

Diane Doolaeghe
Université de Rennes 1
8 PUBLICATIONS **2** CITATIONS
SEE PROFILE

Philippe Davy
French National Centre for Scientific Research
302 PUBLICATIONS **12,417** CITATIONS
SEE PROFILE

Caroline Darcel
65 PUBLICATIONS **1,578** CITATIONS
SEE PROFILE

Romain Le Goc
Itasca Consultants SAS
49 PUBLICATIONS **497** CITATIONS
SEE PROFILE

Some of the authors of this publication are also working on these related projects:

Project HM rock mass behavior characterization View project

Project Fracture density variability View project

All content following this page was uploaded by Philippe Davy on 08 September 2021.

The user has requested enhancement of the downloaded file.

Assessing multiscale Discrete Fracture Network flow with graphs

Doolaeghe, D. and Davy, P.
Géosciences Rennes, University of Rennes, CNRS, Rennes, France
Darcel, C. and Le Goc, R.
Itasca Consultants SAS, Lyon, France
Hyman, J. D.
Earth and Environmental Sciences Division, Los Alamos National Laboratory, Los Alamos, New Mexico, USA

Copyright 2021 DFNE, ARMA

This paper was prepared for presentation at the 3rd International Discrete Fracture Network Engineering Conference held in Houston, Texas, USA, 23-25 June 2021. This paper was selected for presentation at the symposium by the DFNE Technical Program Committee based on a technical and critical review of the paper by a minimum of two technical reviewers. The material, as presented, does not necessarily reflect any position of ARMA, its officers, or members. Electronic reproduction, distribution, or storage of any part of this paper for commercial purposes without the written consent of ARMA/DFNE is prohibited. Permission to reproduce in print is restricted to an abstract of not more than 200 words; illustrations may not be copied. The abstract must contain conspicuous acknowledgement of where and by whom the paper was presented.

ABSTRACT: We evaluate the use of graphs as a fast and relevant substitute to DFNs. Graphs reduce the DFNs' complexity to their connectivity structure by forming an assembly of nodes connected by edges, to which physical properties, like a conductance, can be assigned. Both the graph architecture (either fracture- or intersection- based) and the edge conductance definition, have an impact on the estimation of flow and transport parameters. The intersection graph brings a reliable description of the flow connectivity but with edge redundancy in fractures with a large number of intersections. As a consequence, the expression of the edge conductances should depend on the number of intersections in the fracture plane. We first introduce some of our previous work which propose a reliable expression of the edge conductance in the case of a pair of intersections. For the intersection graph, a correction on the conductance expression is proposed for fractures with a large number of intersections. Both graphs provide very good estimate of the bulk permeability although they tend to slightly overestimate it when the DFN connectivity increases (~×2) certainly due to fractures with large intersection numbers. We address this issue by analyzing flow simulations on a fracture with multiple intersections. We also propose another way to correct the intersection graph, which consists in removing redundant edges. The method drastically simplifies the intersection graph, which is promising in term of computational time. The bulk permeability is overestimated by a factor of 2.3 but independently of the DFN density and connectivity.

1. INTRODUCTION

Fracture networks constitute the basic support for flow and transport in rock matrices, mostly in crystalline rocks. They are multi-scale systems with a broad distribution of the fracture sizes, commonly represented by a decreasing power-law (Bonnet et al., 2001; Bour et al., 2002). They are characterized by a complex topology (the way fractures connect to each other), which is the very first property to characterize the network flow and transport.

Graphs are structures made of nodes, representing discrete elements, and edges, linking these elements. They have been widely used for the analysis of complex networks (Albert and Barabási, 2002) and recently gained attention in the field of fracture network modeling (Hyman et al., 2018; Valentini et al., 2007). They simplify the fracture network but keep its important topology and the hierarchy between fractures.

A challenge in fracture network modeling is to efficiently include the large number of fractures that contribute to flow and transport. Due to the power-law size distribution, fracture networks contain a large number of small fractures that it is difficult to overlook a priori (Bour and Davy, 1997; Davy et al., 2006). Flow and transport simulations using a discrete representation of the fractures, i.e. DFNs (*Discrete Fracture Networks*; Davy et al. (2018)) are thus often computationally heavy. Several recent studies have proposed to use a graph representation of the DFN to simplify the flow and transport simulations, for example, to compute particle breakthrough times (Karra et al., 2018) or perform sensitivity analyses (e.g. multi-level Monte-Carlo; Berrone et al. (2020); O'Malley et al. (2018)). In this case, the graph can provide an estimate of the flow distribution in the network provided that the edge conductances are correctly set.

The present study continues the work of Doolaeghe et al. (2020), in which new estimates of edge conductances have been proposed relying on the geometry of the flowing surfaces of fractures with constant transmissivities. A novelty compared to previous definitions is the dependency of conductances with fracture size. We have applied the edge conductance model to both the fracture graph, in which nodes represent fractures and edges connect two intersecting fractures, and the intersection graph, in which nodes represent intersections and edges connect two intersections of the same fracture (Fig. 1). Flow is then directly computed on these graphs and compared to complete (i.e., meshed) DFN simulations. The results indicated good agreements between graph and DFN, with a maximum difference of a factor of ~2 for highly connected and large DFN. However, recurrent biases are observed for fractures with many intersections, where the a priori estimate of edge conductance is not trivial. First, we propose here a synthesis of our previous work (section 2) and, then, we provide new developments to better adapt the graphs to the DFN complexity. We study how the edge conductances can be adapted in fractures with high intersection numbers (section 3). Finally, we explore a new method that directly removes edges from the intersection graph to avoid its redundant architecture (section 4).

2. ESTIMATING DFN FLOW WITH GRAPHS

2.1. Numerical methods and metrics

The *DFN.Lab* software (Le Goc et al., 2019) is used to simulate flow on the complete meshed DFN and the equivalent graph. DFNs are generated in cubic systems with permeameter boundary conditions. We refer to Karra et al. (2018) for computational details on graph flow solving. In short, heads (m) are calculated at each node by solving the flow conservation. Then, edge flows Q ($m^3.s^{-1}$) are deduced head difference Δh between the edge adjacent nodes and the edge conductances C ($Q = C.\Delta h$). Before solving flow, we extract the DFN and graph backbones, i.e., we remove clusters that are not connected to the two fixed-head boundaries and dead ends (vertices with one neighbor are removed iteratively).

The flow metrics used to compare graph and complete simulations are the system scale equivalent conductivity K ($m.s^{-1}$), and the fracture scale total flow, Q_f ($m^3.s^{-1}$) (Maillot et al., 2016):

$$Q_f = \frac{1}{2}.\sum_{i \in f} |Q_{f,i}| \qquad (1)$$

where $Q_{f,i}$ is the flow exchanged through the i^{th} intersections of the fracture. We refer the reader to Doolaeghe et al. (2020) for descriptions of how to compute K and Q_f.

2.2. Graph architectures

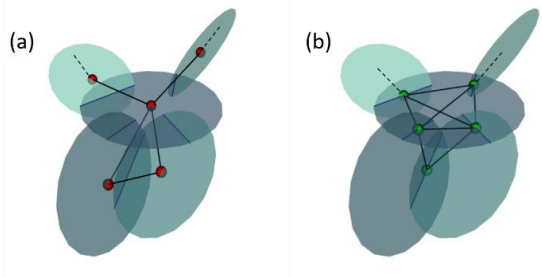

Fig. 1. DFNs and equivalent graphs: (a) fracture graph, (b) intersection graph.

We present in this section the two graph types and how their architecture can introduce some biases in the flow estimations. In the fracture graph, there is one node per fracture and one edge per intersection (Fig. 1,a). This means that all the edges connected to a given fracture share the same fracture node, which results in zeroing the head gradients within the fracture. As a consequence, the fracture graph considers the case of two fractures connected to a third one as a dead-end (i.e., without flow), while there is flow in the full 3D model as shown in

Fig. 2.

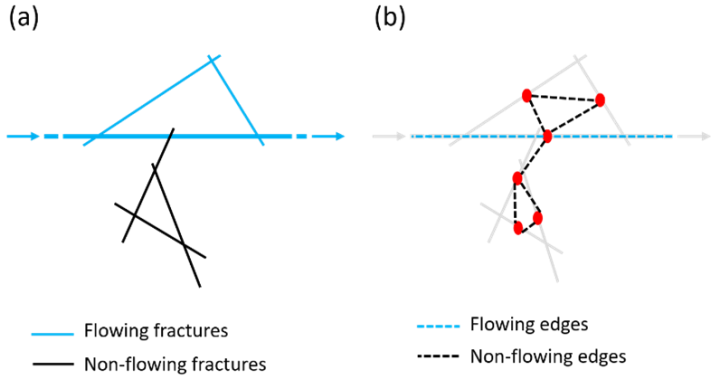

Fig. 2: (a) Two-dimensional representation of fractures and (b) equivalent fracture graph. The fracture configuration aims at showing how some fractures can flow in the complete simulation but not in the fracture graph.

In the intersection graph, nodes are placed on each intersection and they are linked if they belong to the same fracture (Fig. 1,b). The advantage of this configuration is that one can include the direct distance between intersections in the edge properties, which best represents the flowing distance. The disadvantage is that it connects the $\frac{N(N-1)}{2}$ pairs of intersection on a fracture, with N the fracture intersection number, which is likely overestimating the number of 3D flow paths for large N (

Fig. 3,a). If the conductances are calculated as the 2-intersection case problem, this results in an overestimation of the fracture transmissivity due to the multiple paths that link intersections to each other (

Fig. 3,b). In Doolaeghe et al. (2020), a solution was proposed that consists of reducing the conductance of all edge on a fracture by a function of the fracture number of intersection N:

$$\hat{C} = \frac{C}{N-1} \quad (2)$$

In the fracture graph, a unique path exists between all intersections of a fracture, so that such a correction is not necessary. The correction of Eq. (2) can be seen as a way to weight edges so that their weighted sum is equal to the number of edges in the fracture graph, i.e. to $N/2$ edges per fracture.

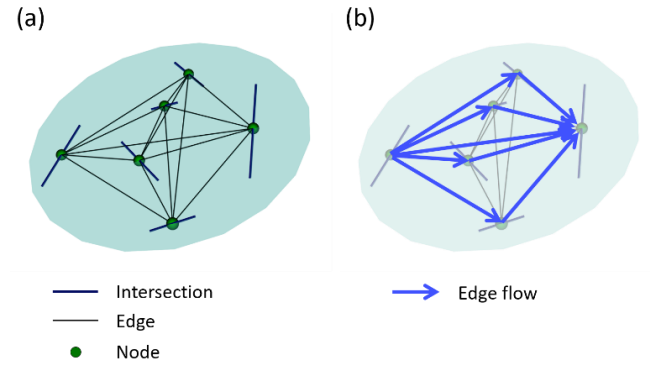

Fig. 3. (a) Fracture with numerous intersections and equivalent intersection graph, showing a significant edge redundancy. (b) resulting edge flow.

2.3. Edge conductance

To calculate the edge equivalent conductance between two fractures or two intersections, we approximate the flow geometry by two trapezoids in series leaning on the fracture intersection(s) and diameter (Fig. 4). We then derived an expression of the equivalent conductance C For the fracture graph (Fig. 4,a), C is:

$$C = \left(\frac{x_1 * \ln\left(\frac{l}{D_1}\right)}{T_1 * (l - D_1)} + \frac{x_2 * \ln\left(\frac{l}{D_2}\right)}{T_2 * (l - D_2)} \right)^{-1} \quad (3)$$

with D_1 and D_2 being the two fracture sizes, T_1 and T_2 the two fracture transmissivities, x_1 and x_2 the distance between the two fracture centers and the intersection center, l the intersection size. For the intersection graph (Fig. 4,b), C is:

$$C = \frac{2.T}{x} * \left(\frac{\ln\left(\frac{D}{l_1}\right)}{(D - l_1)} + \frac{\ln\left(\frac{D}{l_2}\right)}{(D - l_2)} \right)^{-1} \quad (4)$$

with l_1 and l_2 being the two intersection sizes, x the distance between intersections, T and D the fracture transmissivity and size. Note that we use the direct distance between intersections.

In the intersection graph, it is possible to adjust the conductance in the case where the intersections are close, so that the flowing surface is smaller (Fig. 4,c). Instead of the fracture size D, a smaller value d can be used:

$$d = \frac{l_1 + l_2}{2} + B.x \quad (5)$$

where B is a coefficient that we adjusted to 1.5 based on flow simulation between two intersections. In Eq. (4), we replace D by d if $D > d$. We refer to Doolaeghe et al. (2020) for more details about the developments.

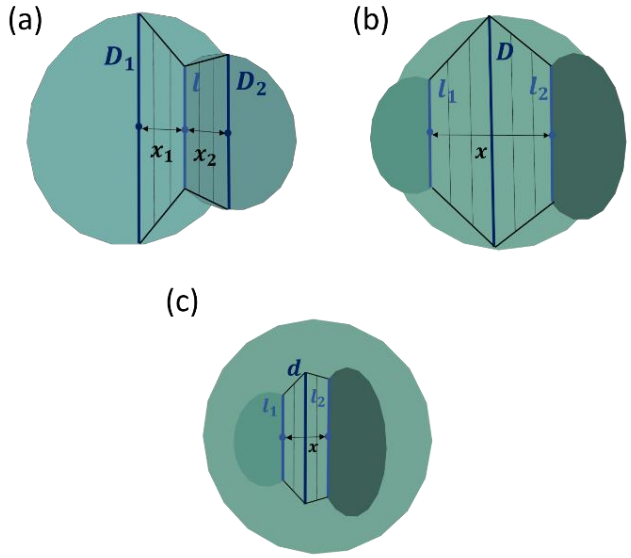

Fig. 4. Schematical representation of the flowing surface using trapezoids. (a) Fracture graph conductance. (b) Intersection graph conductance. (c) Intersection graph conductance with close intersections. Modified from Doolaeghe et al. (2020).

The analytical conductance between two intersections, developed in Eq. (4) and Eq. (5), was compared to a conductance deduced from a complete simulation of the flow between two intersections ($C_{num} = \frac{Q}{\Delta h}$) (Fig. 5.a). Several intersection sizes were evaluated (0.5, 0.3, and 0.1 for a fracture size equal to 1) and the intersections were placed randomly on the fracture, with the exception that they cannot cross. In total, 100 realizations were performed for each intersection size. In Fig. 5.b, the averaged ratio between the analytical conductance C_{th} and the conductance of the complete simulations C_{num} is represented as a function of the distance between intersection centers.

The results indicate a good agreement between the analytical conductance and the flow simulations (thick lines). When the intersections are close, the ratio decreases (~0.8), and the standard deviation is larger possibly due to an effect of the angle between the two intersections. The comparison is also performed for another definition of the conductance (Karra et al., 2018): $C = \frac{(l_1+l_2)}{2x}$ (dashed lines). In this case, the flow is under-estimated, in particular when the intersection sizes are small relatively to the fracture size (blue dashed line),

which indicates the importance of considering the fracture size in the formulation.

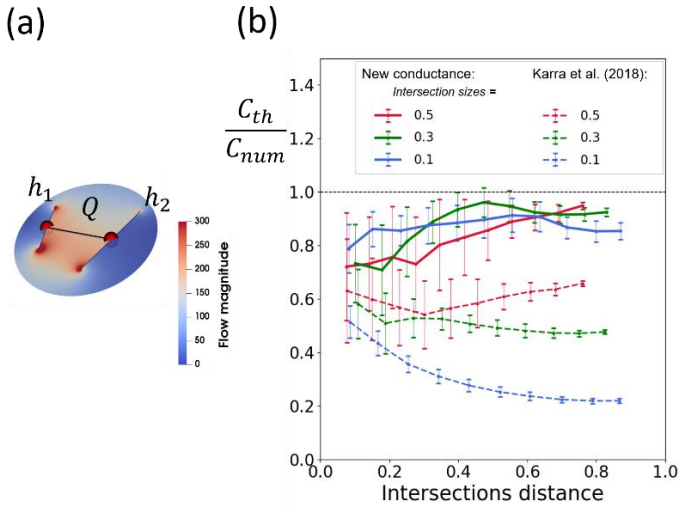

Fig. 5. (a) Numerical simulation of the flow ($m^3.s^{-1}$) between two intersections with fixed head boundary conditions. (b) Ratio between analytical and completely solved conductances as a function of intersection distance. Modified from Doolaeghe et al. (2020).

2.4. Graph flow in multi-scale DFN

The method has been tested on DFN models with a large fracture number. In this manuscript, we present results for DFNs with constant fracture size and DFNs with a power-law size distribution: $n(l) = \alpha.l^{-a}$ (Table 1). Orientations and positions are uniforms. The measure of DFN density is the percolation parameter p (Bour and Davy, 1998), which also quantifies the degree of connectivity (de Dreuzy et al., 2000). All the DFN are above the percolation threshold ($p \sim 2.5$ for randomly oriented disks) and 20 realizations are performed for each percolation parameter.

Table 1: DFN generation parameters and properties. The fracture numbers, N_f are shown for the maximum tested percolation, $p = 3$, and the minimum, $p = 7$. They are averaged over 20 realizations. Modified from Doolaeghe et al. (2020).

	Constant size DFNs		PL size DFNs	
Cubic system size	50		50	
Fracture size, l	3		[1,50]	
PL exponent, a	-		4	
Percolation parameter, p	[3,4,5,6,7]		[3,4,5,6,7]	
	$p = 3$	$p = 7$	$p = 3$	$p = 7$
Fracture number, N_f	11750	27450	33050	73050
N_f in backbone	8000	27100	2200	42950

Fig. 6 and Fig. 7 present the ratio of permeabilities computed from the graphs, K_G, and from the complete 3D simulation, K_{DFN}. For the DFNs with constant fracture size, both the fracture graph (Fig. 6, squares) and the intersection graph with the conductance correction of Eq. (2) (full triangles) give a very good estimate of permeability. Without this correction, the permeability is overestimated by the intersection graph (empty triangles). In the case of DFNs with power-law size distribution (Fig. 7), the permeability is slightly overestimated by both graph methods when the percolation parameter p increases, with differences up to a factor ~ 2 for $p = 7$. This effect is likely due to some large fractures in the highly connected DFNs, whose edge conductance overestimates the actual flow on the fracture plane. We discuss this effect in section 3.

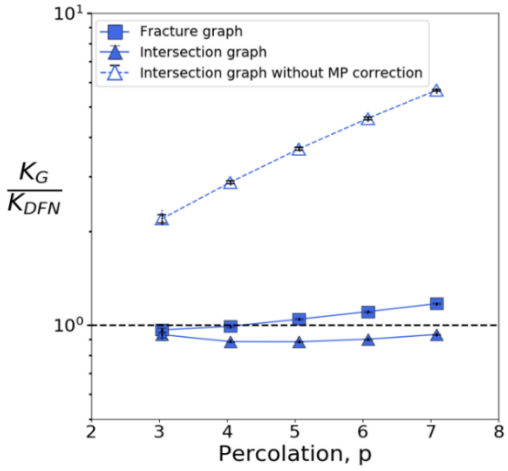

Fig. 6: Ratio of graph permeability, K_G, and complete simulation permeability, K_{DFN}, as a function of the percolation parameter p, in DFNs with constant fracture size. Modified from Doolaeghe et al. (2020).

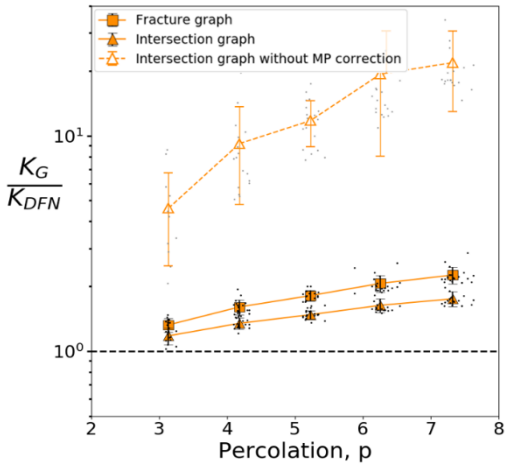

Fig. 7: Ratio of graph permeability, K_G, and complete simulation permeability, K_{DFN}, as a function of the percolation parameter p, in DFNs with PL size distribution. Modified from Doolaeghe et al. (2020).

The flow distribution in the DFN is also analyzed by comparing the flow by fracture Q_f calculated with both

methods (Eq. (1)). Fig. 8 presents an example of comparison for a realization with power-law size distribution and p = 5. On average, there is a rather good agreement between the graph method and the 3D simulation with a limited dispersion around the line $y = x$. An important bias is however observed for the fracture graph where many fractures are dead-ends (no flow) in the graph while flowing in the 3D simulation (red bottom right patch). This is a result of the fracture graph architecture as described in section 2.2. If one would use the graph flow estimations to prune the DFN, e.g. keeping fractures with flows above a given threshold (Srinivasan et al. (2018)), it is thus better to use the intersection graph.

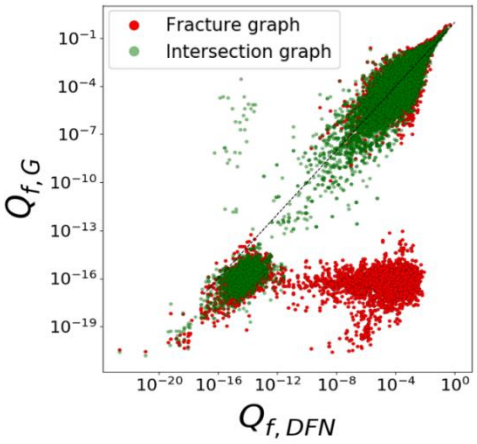

Fig. 8: Flow by fracture comparison between graphs ($Q_{f,G}$) and complete simulation ($Q_{f,DFN}$). Results from one realization of DFN with power-law size distribution and p = 5. The dashed line corresponds to $y = x$. Modified from Doolaeghe et al. (2020).

3. ADAPTING THE EDGE CONDUCTANCE TO MANY INTERSECTIONS

In this section, we present new results to evaluate the conductance of fractures with many intersections in order to address the issue of permeability overestimation.

3.1. Numerical set-up

We use the same numerical set-up as in section 2.3, where the flow is calculated in the fracture plane from one intersection to many others (Fig. 8). A chosen number N of intersections, all having a chosen size l_I, are generated randomly with the condition that they do not cross each other. One intersection is the source with a fixed head h_1, and all the others are sinks with the same fixed head h_2. With this set-up, no flow is possible between the intersection sinks. This enables to compute numerically the equivalent conductance between the source and all the sinks: $C_{num} = \frac{Q_I}{h_2 - h_1}$, with Q_I the flow measured on a sink intersection.

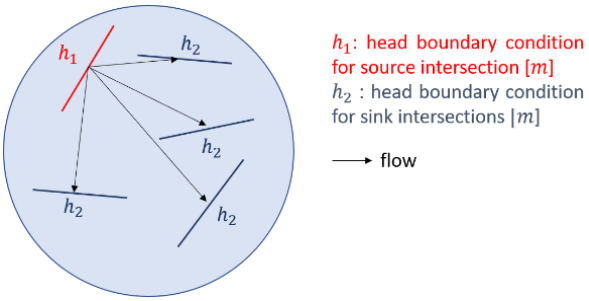

Fig. 9: Numerical set-up used for the flow computation between many intersections on the fracture plane.

3.2. Results

The analytical conductances C_{th} (Eq. (4) and Eq. (5)) is plotted as a function of C_{num} for two intersection sizes: $l_I = 1/4$ (Fig. 10,a) et $l_I = 1/8$ (Fig. 10,b). For each intersection number N, several realizations are computed. When N = 2, C_{num} is well estimated by C_{th}, but when N increases C_{th} overestimates C_{num}. Interestingly, it seems that C_{th} overestimates C_{num} by an additional term that would depend on N:

$$C_{num} = C_{th} - F(N) \quad (6)$$

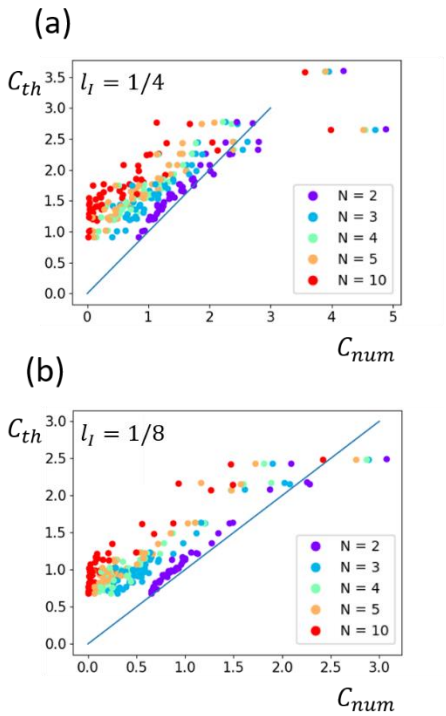

Fig. 10: C_{th} vs C_{num} for several simulations with N intersections of same size l_I. (a) $l_I = 1/4$ and (b) $l_I = 1/8$. The fracture size is 1. The blue line corresponds to $y = x$.

We explore this term $F(N)$ by plotting it as a function of intersection distance (Fig. 11). For each N, linear regressions are performed (straight lines). The results indicate that $F(N)$ is nearly the same independently of the distance between intersections and the intersection sizes l_I.

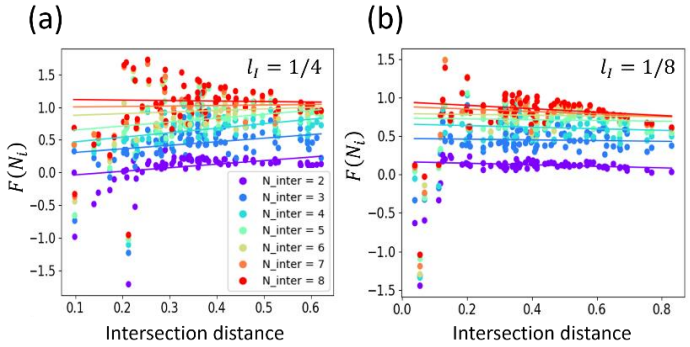

Fig. 11: $F(N) = C_{th} - C_{num}$ as a function of intersection distance. (a) $l_l = 1/4$ and (b) $l_l = 1/8$.

We propose some developments to evaluate this term $F(N)$ as a function of N. The total flow in the complete simulation Q_{tot} can be expressed as:

$$Q_{tot} = \sum_{i}^{N-1} C_{num,i} \,.(h_2 - h_1) \tag{7}$$

with $N-1$ the number of sink intersections. As the term $F(N)$ is the same for all sink intersections, Eq. (6) can be written as :

$$\sum_{i}^{N-1} C_{num,i} = \sum_{i}^{N-1} C_{th,i} - (N-1).F(N) \tag{8}$$

Combining Eq. (7) and (8):

$$F(N) = \frac{1}{N-1}.\left(\sum_{i}^{N-1} C_{th,i} - \frac{Q_{tot}}{|h_1 - h_2|}\right) \tag{9}$$

We make the hypothesis that Q_{tot} is close to the flow between the source and sink intersection with the highest conductance C_{th}:

$$\frac{Q_{tot}}{h_2 - h_1} \sim \max(C_{th}) \tag{10}$$

Combining Eq. (9) and (10):

$$F(N) \sim \frac{1}{N-1}.\left(\sum_{i}^{N-1} C_{th,i} - \max(C_{th})\right) \tag{11}$$

We correct C_{th} by subtracting $F(N)$. The comparison between the corrected conductance $\widehat{C_{th}}$ and the numerical conductance C_{num} is presented in Fig. 12. Note that if $C_{th} - F(N) < 0$, then $\widehat{C_{th}} = 0\ m^2.s^{-1}$. The results indicate a better agreement whatever N is.

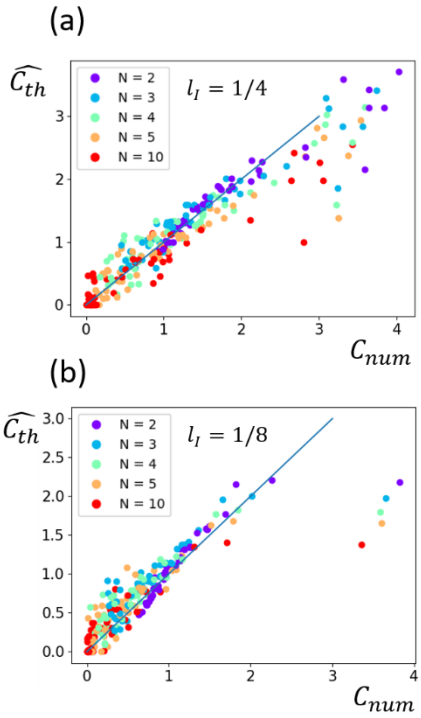

Fig. 12: $\widehat{C_{th}} = C_{th} - F(N)$ vs C_{num}. The blue line corresponds to $y = x$.

The results presented in this section are a first attempt to evaluate the impact of the fracture intersection number on the equivalent conductance. However, it remains limited to the particular head boundary conditions presented in Fig. 9. More work should be done to adapt these results to DFNs, where intersection head configurations are likely to be more complex, with possibly many sources and many sinks intersections, and different heads h_i.

4. MODIFYING THE GRAPH ARCHITECTURE

In this section, we focus on the problem of edge redundancy in the intersection graph. Linking the intersections two by two creates a link network that overestimates the number of flow paths in the fracture (Fig. 13). In addition to creating large biases in the flow estimations, this architecture is computationally expensive because the number of edges increases as N^2 (N is the fracture intersection number) while it varies as N in the fracture graph. In the DFNs with power-law size distribution as those simulated in section 2.4, it is common to find fractures with 100-500 intersections. We propose here a way to simplify the intersection graph architecture.

4.1. Method

The method consists of comparing all pairs of edges on a fracture. If the two edges cross each other, then the one

with the lowest conductance is selected to be removed. The suppression of the selected edges is done after processing all the edges. The method is implemented in the software *DFN.Lab*. Fig. 13 presents an example of fracture with the edges before (a) and after (b) the simplification of the graph. We observe that the number of edges is drastically decreased and none of them intersect anymore, while all intersections are still connected.

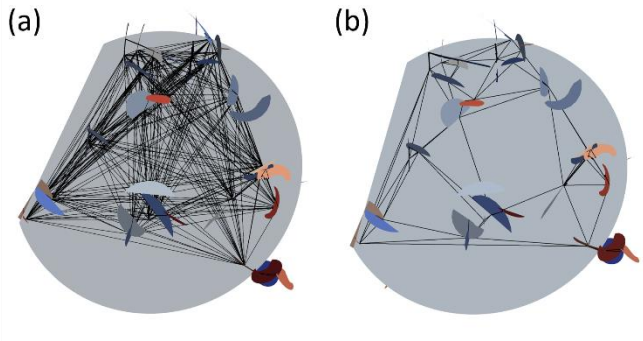

Fig. 13: Isolated fracture from a DFN with intersection graph (black edges). (a) Complete graph. (b) Simplified graph.

4.2. Results

The method is applied on DFNs with power-law size distributions ($a = 4$) and the percolation parameter p is used again as a measure of the fracture density related to DFN connectivity (see section 2.4). Fig. 14 presents the number of edges as a function of the number of intersections per fracture in two DFN realizations with $p = 4$ and $p = 7$. In both cases, the number of edges is about two times the intersection number, which drastically simplifies the intersection graph.

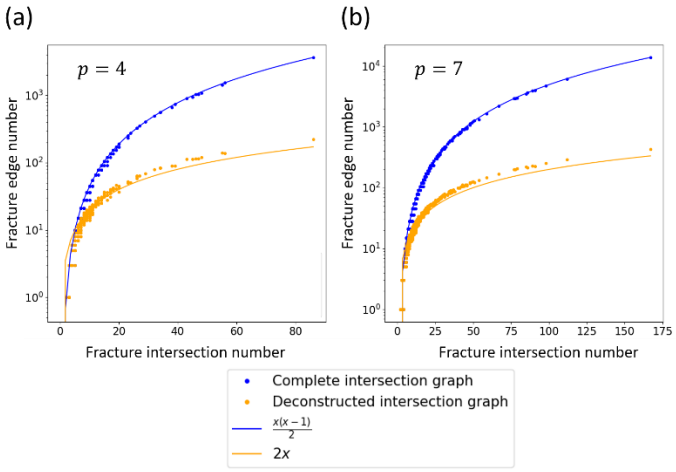

Fig. 14: Edge number (in the intersection graph) vs intersection number per fracture in one DFN realization with power-law size distribution. (a) $p = 4$, (b) $p = 7$.

Fig. 15 presents the equivalent permeabilities obtained with this method. Note that, here, we do not use the edge conductance correction of Eq. (2). After simplifying the graph, the permeabilities are less overestimated than without simplification (see sections 2.2 and 2.4) and the overestimation factor is almost constant around 2.3, independently of the fracture density. If this bias is the same whatever the DFN geometry, it should be easy to correct the permeability after the graph simulation using this method. Further work should focus on how this value could change with other realization types: different size distribution, larger system size, etc. The flowing structure is also evaluated by comparing the Q_f values (Fig. 16).

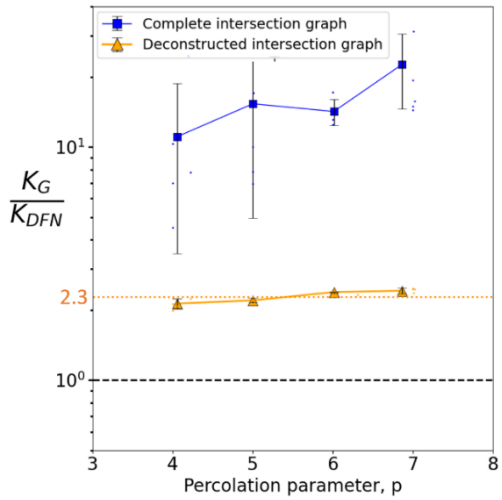

Fig. 15: Ratio of intersection graph permeability, K_G, and complete simulation permeability, K_{DFN}, as a function of the percolation parameter p, in DFNs with PL size distribution.

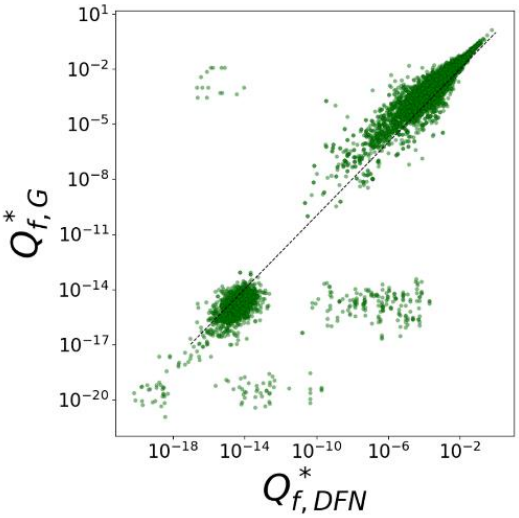

Fig. 16: Flow by fracture comparison between simplified intersection graphs ($Q_{f,G}$) and complete simulation ($Q_{f,DFN}$). Results from one realization of DFN with power-law size distribution and p = 5. The dashed line corresponds to $y = x$.

In Table 2, flow simulation CPU times are provided for the complete simulation and the different graphs. The best speed-up, i.e. ratio of is for the fracture graph, followed by the simplified intersection graph (~10^2). Note that, when simplifying the intersection graph architecture, the algorithm, as it is now, is quite time-consuming. Further work should focus on methods to optimize it.

Table 2: Flow simulation times (in seconds) in graphs and complete simulation, and speed-ups (ratio of complete over graph simulation). The results are indicated for the maximum tested percolation ($p = 3$) and the minimum ($p = 7$) for DFN with power-law size distribution. The numbers are averaged over 20 realizations.

	$p = 3$	$p = 7$
Complete simulation (mesh+flow) (s)	15	300
Fracture graph flow (s)	0.07	2.5
Complete intersection graph flow (s)	0.3	12
Simplified intersection graph flow (s)	0.1	5
Fracture graph speed-up	200	120
Complete intersection graph speed-up	50	25
Simplified intersection graph speed-up	150	60

5. CONCLUSION AND DISCUSSION

In this paper, we have evaluated the use of graphs as surrogate models to solve quickly flow in DFN models. This work is the continuation of a previous one, where we proposed a new expression for conductances that correctly predict flow in the case of pairs of intersections.

Two common types of graph architectures were analyzed: a graph of fractures and a graph of intersections (see Fig. 1). The graph of fractures presents the disadvantage to not reproduce correctly the complete flowing structure, because all edges must connect to a unique position on the fracture plane, creating artificially "dead-loops" (Fig. 2). However, it has the advantage to make good permeability predictions with the proposed expression of edge conductance. Also, it presents the best CPU time speed-ups compared to the complete simulation (Table 2). On the contrary, the intersection graph gives a reliable description of the flow connectivity structure but has the issue of a very high edge redundancy on fractures with a large intersection number (Fig. 3). This induces flow overestimations for highly connected networks. Also, the high number of edges can make the method computationally heavy if it is used on larger DFNs.

Different possibilities to correct the intersection graph are proposed. The first possibility is to reduce all the edge conductances on a fracture by a factor equal to the number of intersections minus one (Eq. (2)). This method presents satisfying results with good permeability and fracture flow predictions. We study the case of a single fracture with a large number of intersections (section 3) randomly positioned. Although the model with one source and several identical sinks is very simple and far to represent what happens in large fractures, the analysis already provides some first insights on how the flow is partitioned in the fracture plane and the implication for finding a reliable estimate of edge conductances.

We also propose another way to address this issue by removing edges from the graph, preferentially edges that are not representative of flow paths. To do so, we assume that, if two edges are crossing, the main flow is in the direction of the edge with the largest conductance, and remove the other (see section 4). The method reduces drastically the edge number in the intersection graph. It provides an estimate of the bulk permeability larger than the reference permeability by a factor independent of the fracture density and DFN connectivity (here ~2.3). More accuracy could be obtained by removing edges that physically do not represent any flowing paths on the fracture, but the difficulty is to have this information a prior as it depends on the boundary conditions and direction of flow within each fracture.

6. ACKNOWLEDGEMENTS

This work is partly funded by Svensk Kärnbränslehantering AB, the Swedish Nuclear Fuel and Waste Management Company, and the ANRT (CIFRE doctoral grant).

7. SUPPLEMENTAL MATERIAL

Graph flow simulation examples are available at this page: https://fractorylab.org/

8. REFERENCES

Albert, R., and A.-L. Barabási, 2002, Statistical mechanics of complex networks: Reviews of modern physics, v. 74, no. 1, p. 47.

Berrone, S., J. Hyman, and S. Pieraccini, 2020, Multilevel Monte Carlo predictions of First passage times in three-dimensional discrete fracture networks: A graph-based approach: Water Resources Research, v. 56, no. 6, p. e2019WR026493.

Bonnet, E., O. Bour, N. E. Odling, P. Davy, I. Main, P. Cowie, and B. Berkowitz, 2001, Scaling of fracture systems in geological media: Reviews of geophysics, v. 39, no. 3, p. 347-383.

Bour, O., and P. Davy, 1997, Connectivity of random fault networks following a power law fault length distribution: Water Resources Research, v. 33, no. 7, p. 1567-1583.

Bour, O., and P. Davy, 1998, On the connectivity of three-dimensional fault networks: Water Resources Research, v. 34, no. 10, p. 2611-2622.

Bour, O., P. Davy, C. Darcel, and N. Odling, 2002, A statistical scaling model for fracture network geometry, with validation on a multiscale mapping of a joint network (Hornelen Basin, Norway): Journal of Geophysical Research: Solid Earth, v. 107, no. B6, p. ETG 4-1-ETG 4-12.

Davy, P., O. Bour, J.-R. De Dreuzy, and C. Darcel, 2006, Flow in multiscale fractal fracture networks: Geological Society, London, Special Publications, v. 261, no. 1, p. 31-45.

Davy, P., C. Darcel, R. Le Goc, R. Munier, J.-O. Selroos, and D. Mas Ivars, DFN, why, how and what for, concepts, theories and issues, *in* Proceedings 2nd International Discrete Fracture Network Engineering Conference2018, American Rock Mechanics Association.

de Dreuzy, J.-R., P. Davy, and O. Bour, 2000, Percolation parameter and percolation-threshold estimates for three-dimensional random ellipses with widely scattered distributions of eccentricity and size: Physical review E, v. 62, no. 5, p. 5948.

Doolaeghe, D., P. Davy, J. D. Hyman, and C. Darcel, 2020, Graph-based flow modeling approach adapted to multiscale discrete-fracture-network models: Physical Review E, v. 102, no. 5, p. 053312.

Hyman, J. D., A. Hagberg, D. Osthus, S. Srinivasan, H. Viswanathan, and G. Srinivasan, 2018, Identifying backbones in three-dimensional discrete fracture networks: A bipartite graph-based approach: Multiscale Modeling & Simulation, v. 16, no. 4, p. 1948-1968.

Karra, S., D. O'Malley, J. D. Hyman, H. S. Viswanathan, and G. Srinivasan, 2018, Modeling flow and transport in fracture networks using graphs: Physical Review E, v. 97, no. 3, p. 033304.

Le Goc, R., B. Pinier, C. Darcel, E. Lavoine, D. Doolaeghe, S. de Simone, J.-R. De Dreuzy, and P. Davy, DFN. lab: software platform for Discrete Fracture Network models, *in* Proceedings AGU Fall Meeting 20192019, Agu.

Maillot, J., P. Davy, R. Le Goc, C. Darcel, and J.-R. De Dreuzy, 2016, Connectivity, permeability, and channeling in randomly distributed and kinematically defined discrete fracture network models: Water Resources Research, v. 52, no. 11, p. 8526-8545.

O'Malley, D., S. Karra, J. Hyman, H. S. Viswanathan, and G. Srinivasan, 2018, Efficient Monte Carlo with graph-based subsurface flow and transport models: Water Resources Research, v. 54, no. 5, p. 3758-3766.

Srinivasan, S., J. Hyman, S. Karra, G. Srinivasan, and H. Viswanathan, Reduced-Order Models of Discrete Fracture Networks Through Flow-Physics on Graph Representations, *in* Proceedings 2nd International Discrete Fracture Network Engineering Conference, Seattle, 2018, American Rock Mechanics Association.

Valentini, L., D. Perugini, and G. Poli, 2007, The “small-world” topology of rock fracture networks: Physica A: Statistical Mechanics and its Applications, v. 377, no. 1, p. 323-328.

View publication stats